Aust. J. Phys., 1984, **37**, 531–47

Horizontal Wave Number Dependence of Type II Solutions in Rayleigh–Benard Convection with Hexagonal Planform

J. M. Lopez and J. O. Murphy

Department of Mathematics, Monash University,
Clayton, Vic. 3168.

Abstract

The horizontal wave number dependence of the hexagonal planform solutions for the Rayleigh–Benard convection problem, which have a nonzero vertical component of vorticity (type II solutions), has been established. Over the range of wave numbers which support cellular convection, comparisons between the thermal transport characteristics of these cyclonic type solutions and those traditionally obtained from nonlinear investigations of the single horizontal mode equations (type I solutions) have been made. From the numerical results obtained, it is found that the cell aspect ratio which maximizes the heat flux of type II solutions is larger than that for type I solutions, at equivalent parameter values, and that the value of the horizontal wave number giving maximum Nusselt number for type II solutions increases with Rayleigh number and decreases with Prandtl number.

1. Introduction

Nonlinear theoretical studies on cellular convection have not, as yet, been able to satisfactorily resolve one aspect of the problem, namely the determination of the preferred horizontal scales for the cellular motions. Many attempts (see e.g. Toomre *et al.* 1977) have been made to match theoretical predictions with experimental observations; however, these have only been both qualitatively and quantitatively successful when the system is in its marginal state, i.e. just at the onset of convective instability, which is governed by the linearized system of equations (Chandrasekhar 1961; Murphy 1977). This agreement in the linear theory between theoretical and experimental cell sizes is to be expected, since the disturbance will have the scale of the mode which first becomes unstable, and this scale is uniquely defined by the linear theory. The precise relationship between the Rayleigh number R and the horizontal scale of the convective cells in terms of the aspect ratio a (defined as the ratio of the vertical to horizontal dimensions of the convective cell and known as the dimensionless horizontal wave number), when the stress-free boundary conditions apply at both the top and the bottom of the layer, is given by the characteristic equation

$$R = (\pi^2 + a^2)^3/a^2 .$$

When this relationship is plotted in the R–a parameter plane the locus gives the marginal stability curve. In turn the form of this curve is modified by both the nature of the boundary conditions employed for the vertical velocity $W(z)$, as a function of the vertical coordinate z, and the temperature fluctuation $F(z)$, as well

0004-9506/84/050531$02.00

as by the imposition of external constraints such as rotation and a magnetic field. Specifically, the minimum value of R for stress-free boundaries, the case considered throughout this paper, is given by

$$R_c = 657{\cdot}5 \quad \text{with} \quad a_c = \sqrt{\tfrac{1}{2}}\pi,$$

and consequently at the marginal state the disturbances will be characterized by the wavelength

$$\lambda = 2\pi d/a = 2^{3/2}d,$$

where d is the layer depth over $0 \leqslant z \leqslant 1$. For any particular $R = R_0$ and $R_0 > R_c$, the range of values of a governed by

$$\gamma = (\pi^2 + a^2)^3/a^2 R_0 \leqslant 1$$

will support convective motions in the fluid.

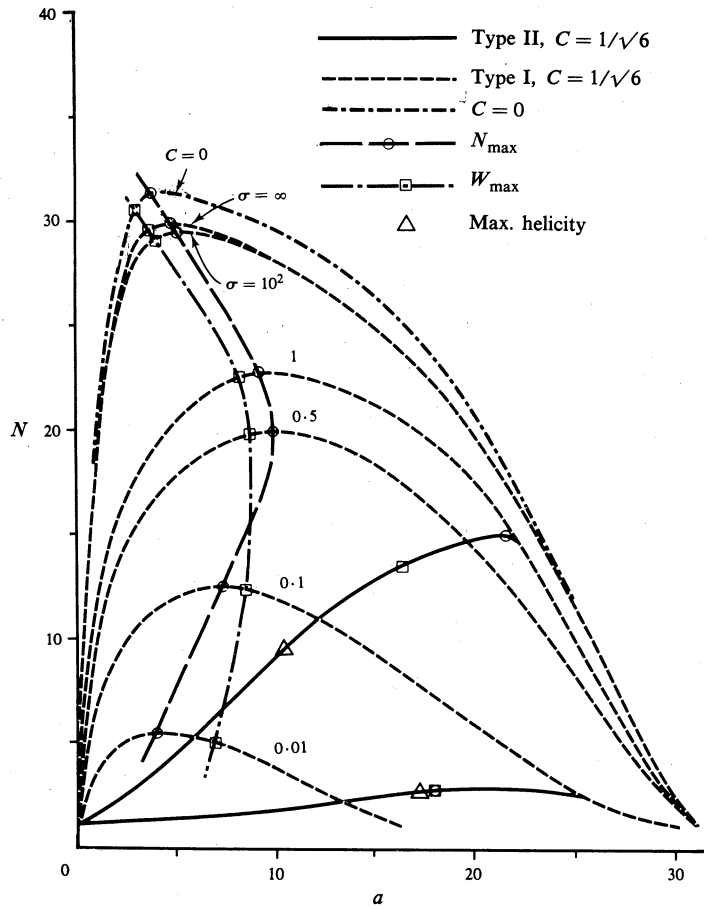

Fig. 1. Variation of the Nusselt number N with aspect ratio a for $R = 10^6$ and the values of σ indicated for type I, type II and mean-field solutions with maximum Nusselt number, vertical velocity and helicity.

In nonlinear studies of cellular convection, utilizing the mean-field equations (Herring 1963), it is found that the range of horizontal wave numbers supporting convective motions in a fluid is also determined by the condition $\gamma \leqslant 1$ and, further, within this range the heat flux as defined by the Nusselt number

$$N = 1 + \int_0^1 FW \, dz$$

reaches a single maximum. However, investigations using the single-mode steady state equations with hexagonal planform, which incorporate additional nonlinear terms in the differential system and the influence of the Prandtl number σ, have demonstrated that for any particular R the range of aspect ratios supporting convective motions is reduced with decreasing Prandtl number. This contraction in the range of a, which cannot be predicted by the linear theory, takes place essentially at the high a end of the range, hence eliminating the narrowest cells that support convection following the mean-field equations. This dependence of N on a and σ is illustrated in Fig. 1 where C takes the value $\sqrt{\frac{1}{6}}$ for hexagonal cells. From the results summarized here, it is evident that the maximum value of N is attained at a value of a which varies with σ and that the maximum value of a for maximum N is attained for $\sigma \approx 0{\cdot}5$.

Convection in Nature exhibits certain preferred length scales. In the Sun, we observe two definite scales of convective motion, granules and super granules with approximate widths of 2000 and 30 000 km respectively; definite cell sizes are also observed in meso-scale convection in the Earth's atmosphere, with cell diameters typically of 30–60 km and depths ranging from 1 to 2 km. Further, the ordered cellular structure observed in laboratory experiments involving fluids with varying Prandtl number is well known from the many excellent published photographs. Although the theory allows the system's disturbances to grow with a wide spectrum of scales, it is clear that only a small number of these is selected.

Malkus and Veronis (1958) presented a 'relative stability' criterion as a possible means to predict which scales of motion would prevail in cellular convection. Basically, it specified that the horizontal wave number which gives the highest heat flux, meaning that at which convection is most efficient, is the one at which the convection will prevail. However, there appears to be no firm physical basis for this stability criterion; further, since it is based on expansions involving a small parameter, which is effectively $(R/R_c - 1)^{\frac{1}{2}}$, it is only valid near the marginal stability regime of the system. Hence, it cannot take into account dynamic instabilities, such as the one illustrated by Lopez and Murphy (1983) where boundary layer instabilities led to the generation of a component of vertical vorticity and a transition to a new stable state. Nevertheless, it is still felt that the fluid will endeavour to transport heat in the most efficient manner, but it will also select the most stable mode which is compatible with efficiency. Murphy and Lopez (1984) demonstrated the existence of a new state which, although being less efficient than the usual state determined by the steady single-mode system of equations with hexagonal planform, has a number of properties rendering it the more stable of the two, and hence probably the preferred state.

Murphy and Lopez (1984) made a detailed examination of this new state, concentrating on the effects of varying the Rayleigh and Prandtl numbers, with a

fixed value of the horizontal wave number, on the steady state system. In the present study, an investigation of the dependence on the aspect ratio is presented. The notation used by Murphy and Lopez (1984) will again be utilized here, and only a brief summary of their physical and mathematical formulation will be presented. With the new type II solutions it is found that the aspect ratio at which the heat flux is maximized is considerably larger than for type I and it increases as the Rayleigh number is increased, whereas the maximizing aspect ratio decreases with the Prandtl number, but is still larger than the corresponding aspect ratio for type I.

2. Equations

As in our previous work (Murphy and Lopez 1984), we investigate the nature of finite amplitude instabilities in a horizontal fluid layer of infinite extent, held between two isothermal stress-free boundaries separated by a depth d, which is heated from below and maintained at a temperature difference of ΔT. The governing equations are the momentum equation

$$\rho\,\partial \boldsymbol{u}/\partial t + \rho \boldsymbol{u}\,.\,\nabla \boldsymbol{u} + \nabla p - \rho \boldsymbol{G} - \mu \nabla^2 \boldsymbol{u} = 0, \tag{1}$$

together with the continuity equation

$$\partial \rho/\partial t + \nabla\,.\,(\rho \boldsymbol{u}) = 0, \tag{2}$$

and the heat equation

$$\rho C_V\,\partial T/\partial t + \rho C_V \boldsymbol{u}\,.\,\nabla T - K\nabla^2 T = 0, \tag{3}$$

where μ, K and C_V are the coefficient of kinematic viscosity, the conductivity and the specific heat at constant volume, $\boldsymbol{G}$ is $(0, 0, g)$, g being the acceleration due to gravity, and $\boldsymbol{u}$, T, P and ρ are the velocity, temperature, pressure and density of the fluid. The fluid is taken to be Boussinesq, so that density fluctuations are solely due to buoyancy effects, and hence the continuity equation (2) reduces to $\nabla\,.\,\boldsymbol{u} = 0$.

The steady state single-mode equations, which employ the following expression for the (non-dimensionalized) velocity

$$\boldsymbol{u} = \left\{\frac{1}{a^2}\left(\mathrm{D}W(z)\frac{\partial f}{\partial x} + Z(z)\frac{\partial f}{\partial y}\right),\ \frac{1}{a^2}\left(\mathrm{D}W(z)\frac{\partial f}{\partial y} - Z(z)\frac{\partial f}{\partial x}\right),\ W(z)f\right\}, \tag{4}$$

are (Murphy and Lopez 1984, equations 11–14)

$$(\mathrm{D}^2 - a^2)Z = (C/\sigma)(W\mathrm{D}Z - Z\mathrm{D}W), \tag{5}$$

$$(\mathrm{D}^2 - a^2)^2 W = Ra^2 F + (C/\sigma)\{W(\mathrm{D}^2 - a^2)\mathrm{D}W + 2\mathrm{D}W(\mathrm{D}^2 - a^2)W + 3Z\mathrm{D}Z\}, \tag{6}$$

$$(\mathrm{D}^2 - a^2)F = W\mathrm{D}T_0 + C(2W\mathrm{D}F + F\mathrm{D}W), \tag{7}$$

$$\mathrm{D}^2 T_0 = \mathrm{D}(FW), \tag{8}$$

where $\mathrm{D} \equiv \mathrm{d}/\mathrm{d}z$, W is the vertical component of velocity, Z is the vertical component of vorticity, T_0 is the mean temperature across the layer, F is the temperature fluctuation, $a = kd$ is the aspect ratio with k the horizontal wave number, $\sigma = \nu/\kappa$ is the Prandtl number which gives the ratio of viscous to thermal diffusivities, and $R = g\alpha d^3 \Delta T/\kappa\nu$ is the Rayleigh number with α the coefficient of volume expansion.

From the linearized system (Chandrasekhar 1961) there exist separable solutions of the form $w(x,y,z) = f(x,y)\,W(z)$, where the function $f(x,y)$ satisfies the two-dimensional Helmholtz equation

$$\frac{\partial^2 f(x,y)}{\partial x^2} + \frac{\partial^2 f(x,y)}{\partial y^2} = -a^2 f(x,y). \tag{9}$$

In this study, we employ the particular solution of equation (9)

$$f(x,y) = (\tfrac{2}{3})^{\frac{1}{2}}\{2\cos(\tfrac{1}{2}\sqrt{3}ax)\cos(\tfrac{1}{2}ay) + \cos(ay)\}, \tag{10}$$

corresponding to a hexagonal planform, which is due to Christopherson (1940). Hence C, the planform constant defined by

$$C = \iint_{\text{cell}} f^3(x,y)\,\mathrm{d}x\,\mathrm{d}y \Big/ \iint_{\text{cell}} f^2(x,y)\,\mathrm{d}x\,\mathrm{d}y, \tag{11}$$

takes the numerical value $\sqrt{\frac{1}{6}}$ in the case of hexagonal convection cells.

Two important numbers characterize the flow, the first of these, the Nusselt number, is the first integral of equation (8), expressed as

$$N = F(z)\,W(z) - \mathrm{D}T_0(z),$$

and gives the ratio of heat transferred by the convective system to that which would have been transferred if the system were immobilized. The second is the helicity, which is only nonzero if the flow has a vertical component of vorticity, and this is defined by

$$H_0 = \iiint_{\text{cell}} \boldsymbol{u}.(\nabla \times \boldsymbol{u})\,\mathrm{d}x\,\mathrm{d}y\,\mathrm{d}z, \tag{12}$$

which in this case takes the form

$$H_0 = \int_0^1 \{\mathrm{D}W(z)\,\mathrm{D}Z(z) - Z(z)(\mathrm{D}^2 - a^2)W(z) + a^2 W(z)\,Z(z)\}\,\mathrm{d}z. \tag{13}$$

Equations (5)–(8) are solved together with stress-free boundary conditions, which state that

$$W(z) = \mathrm{D}^2 W(z) = \mathrm{D}Z(z) = 0$$

on $z = 0$ and $z = 1$. The bounding surfaces are also considered to be isothermal, so that

$$F(z=0) = F(z=1) = 0$$

in conjunction with $T_0(z=0) = 0$ and $T_0(z=1) = -1$.

The method of solution employed is that of truncated Fourier expansions as detailed by Murphy and Lopez (1984), where the variables are expanded in either a sine or cosine series, depending on the boundary conditions, and then substituted into equations (5)–(8) which yields a system of algebraic equations for the coefficients of the expansions, with these being solved by utilizing the generalized Newton–Raphson method.

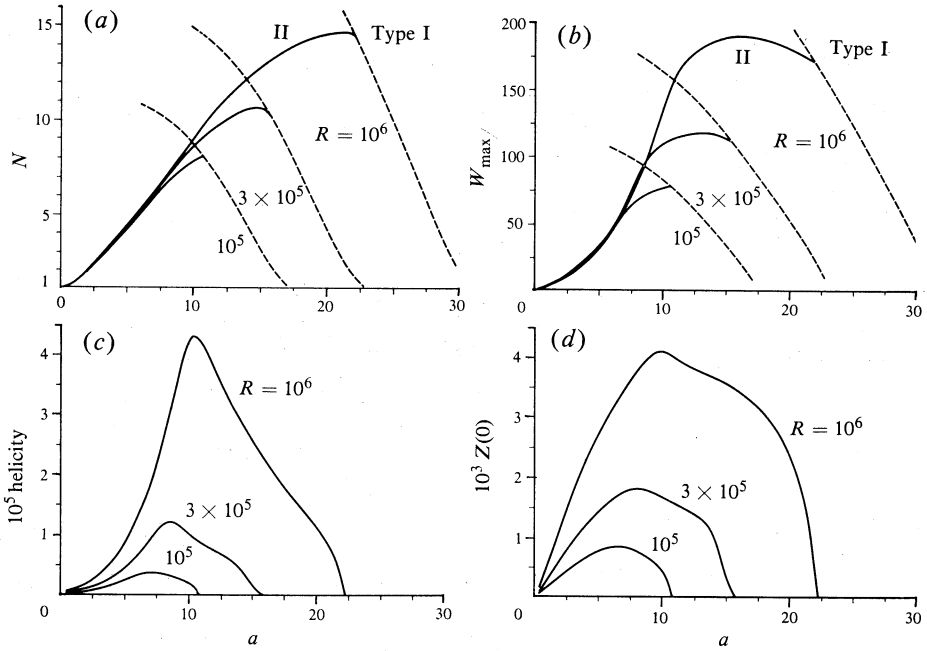

Fig. 2. Variation with aspect ratio a, for $\sigma = 1$, of (a) the Nusselt number N, (b) the maximum vertical velocity W_{max}, (c) the helicity and (d) the vertical vorticity for type I (dashed curves) and type II (solid curves) solutions.

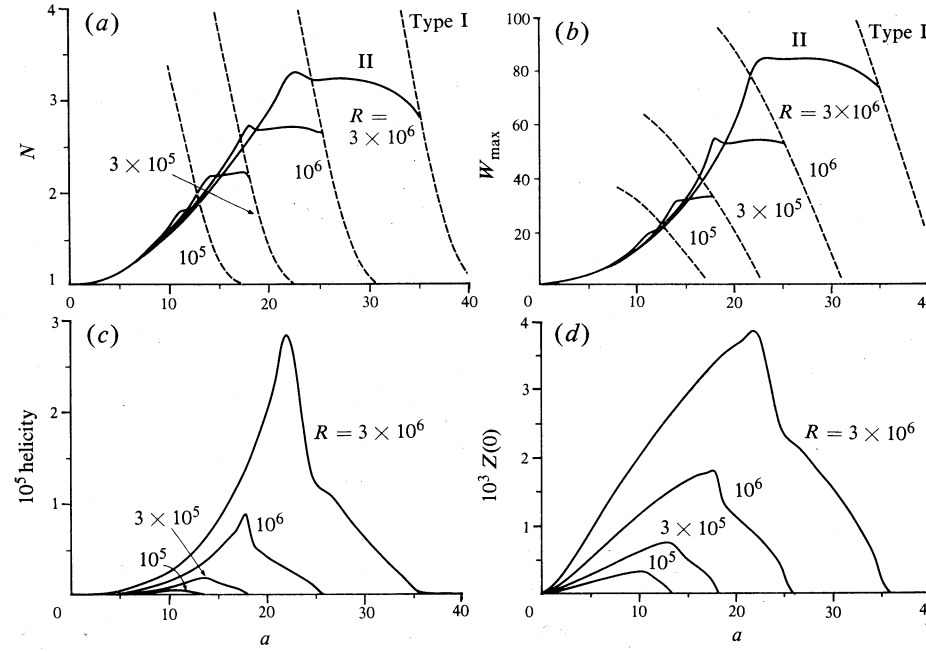

Fig. 3. Variation with aspect ratio a, for $\sigma = 0{\cdot}1$, of (a) the Nusselt number N, (b) the maximum vertical velocity W_{max}, (c) the helicity and (d) the vertical vorticity for type I (dashed curves) and type II (solid curves) solutions.

3. Numerical Results

It has been established by Murphy and Lopez (1984) that when the single-mode nonlinear hexagonal system was solved using the stress-free boundary conditions, two distinct solutions existed for certain ranges of the Rayleigh and Prandtl numbers. It was also concluded that the aspect ratio of the cell would play an important role in determining the physical characteristics of the flow associated with the new type II solutions. This dependence has now been investigated numerically and the results are reported here for the selected parameter values of $R = 10^5$, 3×10^5, 10^6 and 3×10^6 together with $\sigma = 1{\cdot}0$ and $0{\cdot}1$, while the aspect ratio a has been varied over the entire range supporting type II solutions, which is a subrange of that defined by $\gamma \leqslant 1$.

On a comparative basis it is evident from Figs 2*a* and 3*a* that at all values of a for which type II solutions exist, the convective heat flux due to type I is greater than for type II solutions, and at the high end of the range of a which supports type II solutions, type I and type II coalesce. Physically it is quite reasonable that type II solutions do not exist at large a, as this situation corresponds to very narrow cells, and since adjoining vortices would be directed in opposite directions, this would inhibit their generation. The wave number computed for the coalescence of the type I and type II solutions, for any set of parameter values, will be denoted by a_j.

In Figs 2 and 3, the variation of (*a*) the Nusselt number, (*b*) the maximum vertical velocity in the layer, (*c*) the helicity and (*d*) the vertical vorticity at the bottom of the layer—the vertical vorticity always being greatest at the bottom boundary and decreasing monotonically up through the layer—is shown against the aspect ratio for various values of the Rayleigh R and Prandtl σ numbers for the type II solutions. For a range of a values in the vicinity of a_j, the variations of the Nusselt number and maximum vertical velocity with a for type I solutions are also included (dashed curves). The full type I dependence of the Nusselt number and maximum vertical velocity was given by Murphy (1980), and has been summarized here in Fig. 1.

When the Prandtl number is large, say $\sigma > 10$, only type I solutions were found to exist, regardless of the aspect ratio. For $\sigma = 1{\cdot}0$, it can be noted from Fig. 2 that type II solutions exist at low values of a, where $\gamma \leqslant 1$, corresponding in geometric terms to wider convection cells. At small a, the Nusselt number is now independent of the Rayleigh number when σ is fixed (see Fig. 2*a*), and it is only when the type II N–a curve, for a particular value of R, reaches the neighbourhood of a_j that it 'peels' away from the 'asymptotic' R-independent N–a curve. In the case where $\sigma = 1{\cdot}0$, it 'peels' off to lower N values and coalesces with the type I N–a curve, at which point the helicity and vertical vorticity vanish. Also, the values of a at which the type II N–a curves leave the 'asymptotic' curve and those at which the helicity and vertical vorticity reach their maximum appear to coincide for $\sigma = 1{\cdot}0$. The numerical results for $\sigma = 1{\cdot}0$ given in Fig. 2*a* also indicate that the maximum value of the Nusselt number is attained, for each of the three values of R considered, at values of a which are in the vicinity of the respective a_j points. Now assuming that the type II solution is the physically preferred solution [the results from Lopez and Murphy (1983) strongly suggest this to be the case], and using the hypothesis put forward by Malkus and Veronis (1958) that the preferred cell size corresponds to the wave number for maximum heat flux then, when $\sigma = 1{\cdot}0$, one would expect to observe cells exhibiting the characteristics of essentially type I solutions with very

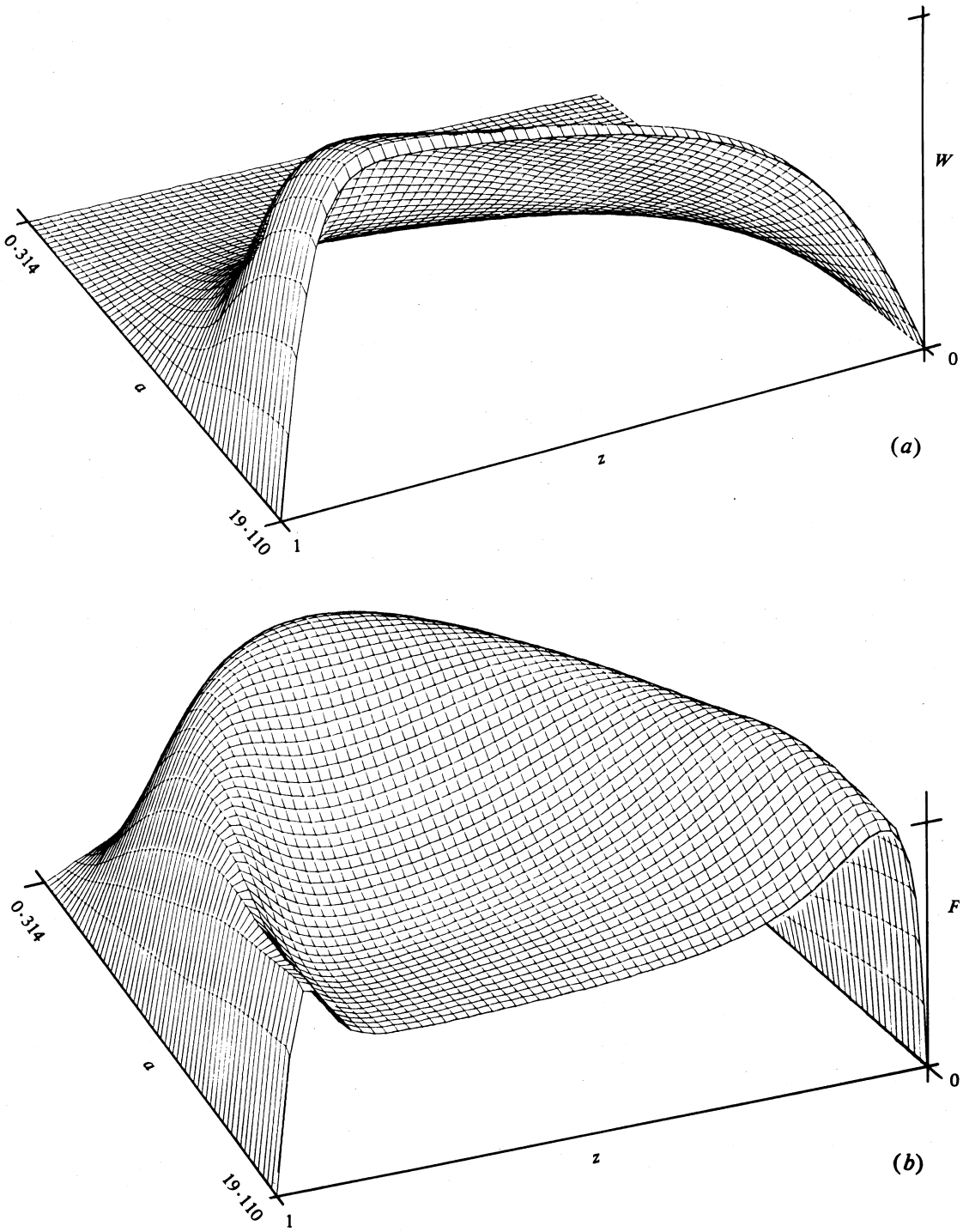

Fig. 4. Variation with aspect ratio a across the fluid layer $0 \leqslant z \leqslant 1$ for type II solutions of (a) the vertical velocity $W(z)$, (b) the temperature fluctuation $F(z)$, (c) the mean temperature profile $T_0(z)$ and (d) the vertical vorticity $Z(z)$. In each case $R = 3 \times 10^5$ and $\sigma = 0{\cdot}1$.

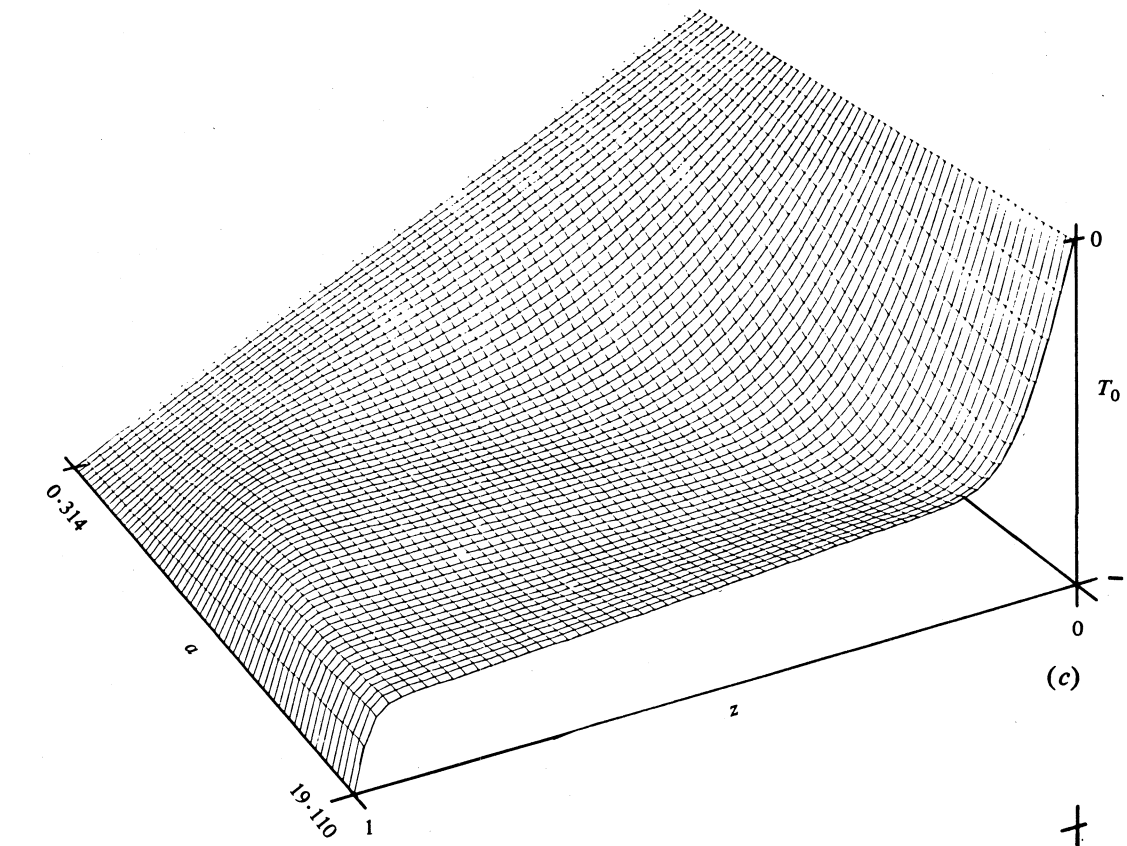

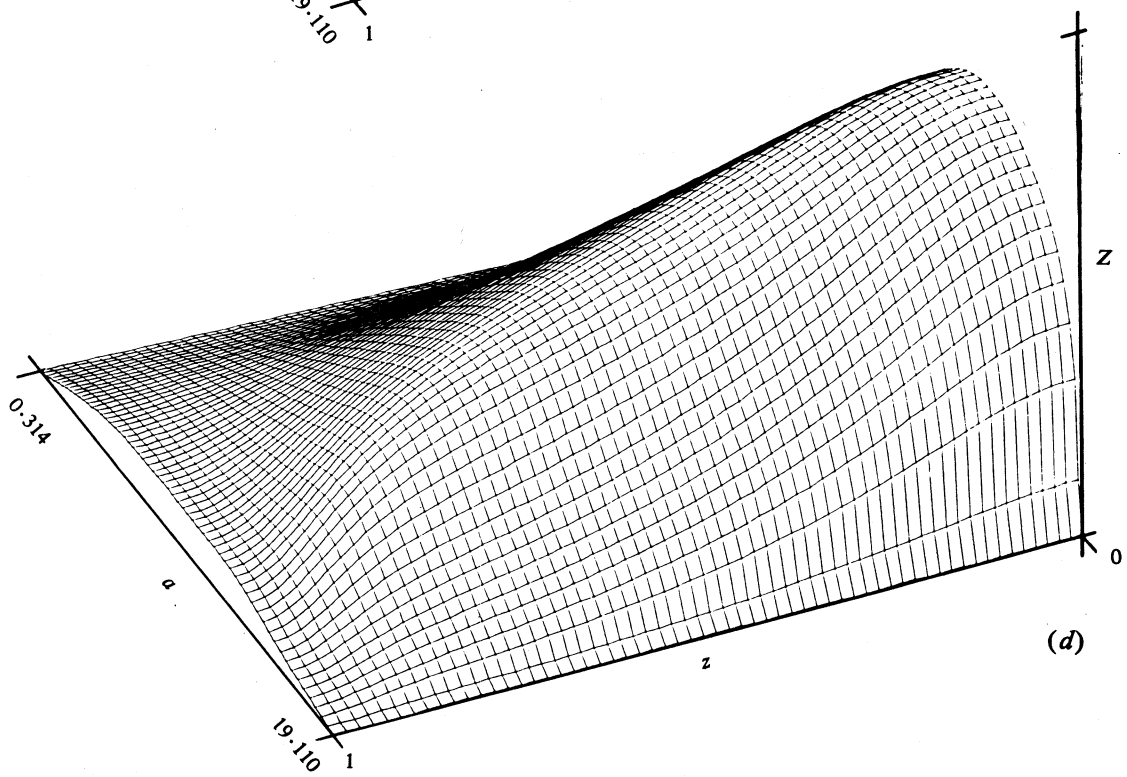

Figs 4*c* and 4*d*.

little helicity. However, the aspect ratio of these cells is larger than that predicted by the single-mode equations which neglect the component of vertical vorticity, designating narrow convection cells at maximum heat flux.

It appears that these $\sigma = 1{\cdot}0$ solutions are also representative of the solutions for all values of $\sigma > 1{\cdot}0$ up to the maximum value of σ associated with type II solutions. The situation, however, changes as one goes to a lower Prandtl number. Fig. 3 shows the corresponding variation of (*a*) Nusselt number, (*b*) maximum vertical velocity, (*c*) helicity and (*d*) vertical vorticity at $z = 0$, against a, for $\sigma = 0{\cdot}1$. Now, the Nusselt number for type II solutions is no longer essentially monotonically increasing with a to a_j, but instead has a well defined maximum, especially for the larger values of R considered, well before a_j is reached. For small a, N is again independent of R when $\sigma = 0{\cdot}1$. However, there now exists a range in a where the convective heat flux for a particular value of R is greater than for all larger values of R, and it is within this range of a that the maximum Nusselt number for the type II solutions occurs. Another interesting feature associated with these values of a for N_{max} is that they correspond to the maximum helicity, vertical vorticity and vertical velocity for each R considered. It is significant that all four are maximized at the same value of a when $\sigma = 0{\cdot}1$. Accordingly, one would then expect this to be the preferred a, which is still larger than that corresponding to N_{max} for type I solutions, but is now associated with a flow possessing both substantial helicity and vertical vorticity. A degree of non-uniqueness is apparent with these nonlinear type II solutions. Specifically, at the particular values of a where any two curves in the N–a parameter space intersect, the same N value is given for at least two different values of R, as illustrated in Fig. 3*a*. An equivalent situation is evident from Fig. 3*b* which gives the W_{max} variation for type II solutions.

The effects of varying the aspect ratio on the physical features of the flow associated with the type II solutions—as depicted by the velocity, vorticity and temperature distributions across the layer—is now considered in detail. In Fig. 4 the profiles of the functions (*a*) $W(z)$, (*b*) $F(z)$, (*c*) $T_0(z)$ and (*d*) $Z(z)$, for $0 \leqslant z \leqslant 1$, for the parameter values $R = 3 \times 10^5$ and $\sigma = 0{\cdot}1$ have been plotted against the aspect ratio in the range $a = 0{\cdot}314$–$19{\cdot}110$. As the aspect ratio is reduced to its lower limit, the profiles of W, F and T_0 all tend towards the conductive state; the W and F profiles are sine curves of very small amplitude and the T_0 profile is a straight line with gradient -1. However, it is surprising to observe that the Z profile which, under normal expectations, should be identically zero near the conductive state, has a definite cosine form in amplitude, with the coefficient $L_0 \neq 0$ (see Murphy and Lopez 1984, equation 16b). At the large a end of the range, which approximates a_j for the transition from separate type I and type II to type I alone, the highly nonlinear nature of both these solutions near a_j is evident. This is manifested most strongly in the W, F and T_0 profiles while, in contrast, the Z profile which prototypes the type II solutions rapidly vanishes. We have undoubtedly established that at large a type I and II solutions coalesce, whereas there was no evidence of any comparable behaviour at low a; even at very small a the type I and II solutions retained their separate identities. The vertical vorticity at low a, relative to the vertical velocity, was always nonzero provided it was also nonzero at some larger values of a for the same R and σ values. In general, the Z profile given in Fig. 4*d* shows that near the bottom of the layer the vertical vorticity is

quite large, that it gradually diminishes up through the layer, and that within the upper section of the fluid layer an abrupt reduction takes place.

The boundary conditions adopted for $W(z)$ dictate that there be no flow normal to the top boundary, and hence it is practical to plot the streamlines of the flow at this level and demonstrate the effects of different aspect ratios on the cellular flow pattern for type II solutions. These are given in the sequence of Fig. 5 for $R = 10^6$, $\sigma = 1{\cdot}0$ and for the various values of a indicated. A more complete representation of the convective motions is obtained when these flow patterns are viewed in conjunction with Fig. 6, where the vector projections of the velocity (*top*) and vorticity (*middle*) together with contours of their strength, given respectively by contours of $|\boldsymbol{u}|$ and $|\nabla \times \boldsymbol{u}|$, as well as the corresponding isotherms (*bottom*), are plotted in the x–z plane at the y values indicated for nine values of a. It is not possible to draw streamline representations in the x–z plane because there are components of velocity normal to it. At low a Figs 5*a* and 6*a* show that the flow is almost entirely horizontal. However, there must be some vertical flow as the vorticity does show some horizontal components and the Nusselt number is greater than one. In addition, Fig. 5*a* reveals the tops of some very strong vortices; the large ones which are situated at the centre of the individual cells, such as that at $(x, y) = (0, 0)$, are directed upwards and are surrounded by six weaker ones, located at the vertices of the hexagonal cells and directed downwards. The nature of the isotherms at this small aspect ratio reflects the small vertical velocity associated with the type II flow, in that they are mostly horizontal with an upwelling in the centre of the cell, together with comparable downdrafts at the vertices. Overall a near linear temperature gradient persists.

When the aspect ratio is increased to about $a = 3$ or 4, the manner in which the flow spirals upwards through the vortex in the centre of the hexagonal cell and then flows into the downward vortices at the vertices is readily observed from Figs 5*b* and 5*c* and Figs 6*c*–6*e*. The isotherms indicate the development of plumes of hot fluid rising in the centre and cooler fluid descending at the vertices.

At $a \approx 5$ one finds, from Fig. 6*f*, the flow developing circulation currents near the top of the layer, so that in the x–z plane the velocity vector projections are no longer all directed in the negative x direction, indicating that the flow is no longer purely clockwise inside the cell. The corresponding streamlines in Fig. 5*d* indicate a reduced amount of swirling at the top of the layer, but still show how the flow helixes up the central region of the cell and descends down the vortices at the vertices of the cell. The isotherms show the development of extended isothermal regions in the layer.

Fig. 6*g* demonstrates that for $a \approx 7$ the circulatory motion has now extended considerably deeper into the layer, the vertical vorticity is concentrated essentially in the central base of the cell, where the twisting is strongest, and also, as indicated by Fig. 5*e*, the vertical vorticity at the top of the layer is almost zero, with the streamlines showing very little twisting at the top of the layer. The isothermal region now is also very well defined. At $a \approx 10$ as in Fig. 6*h*, which coincides with maximum helicity and vertical vorticity at the bottom of the layer, this behaviour is even more pronounced; the streamlines plotted in Fig. 5*f* are now almost radial, indicating that the vertical vorticity is almost zero there. When $a \approx 17$ as in Fig. 6*i*, the flow is now virtually typical type I (see Fig. 7) for a large aspect ratio at $\sigma = 1{\cdot}0$, with a thin viscous boundary layer at the top and extended central isothermal region.

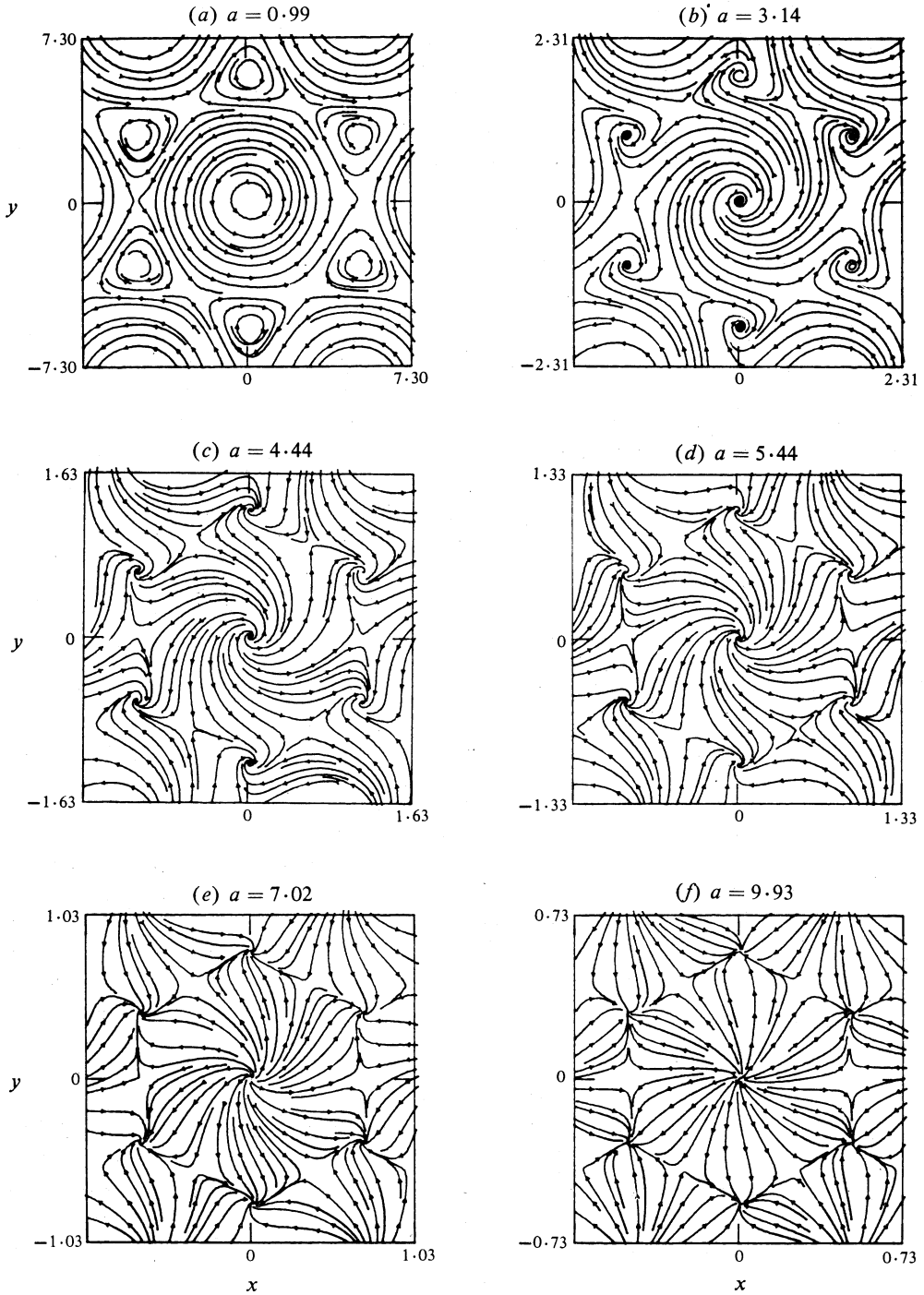

Fig. 5. Velocity streamlines at the top of the layer for type II solutions, for $R = 10^6$, $\sigma = 1{\cdot}0$ and the six values of a indicated.

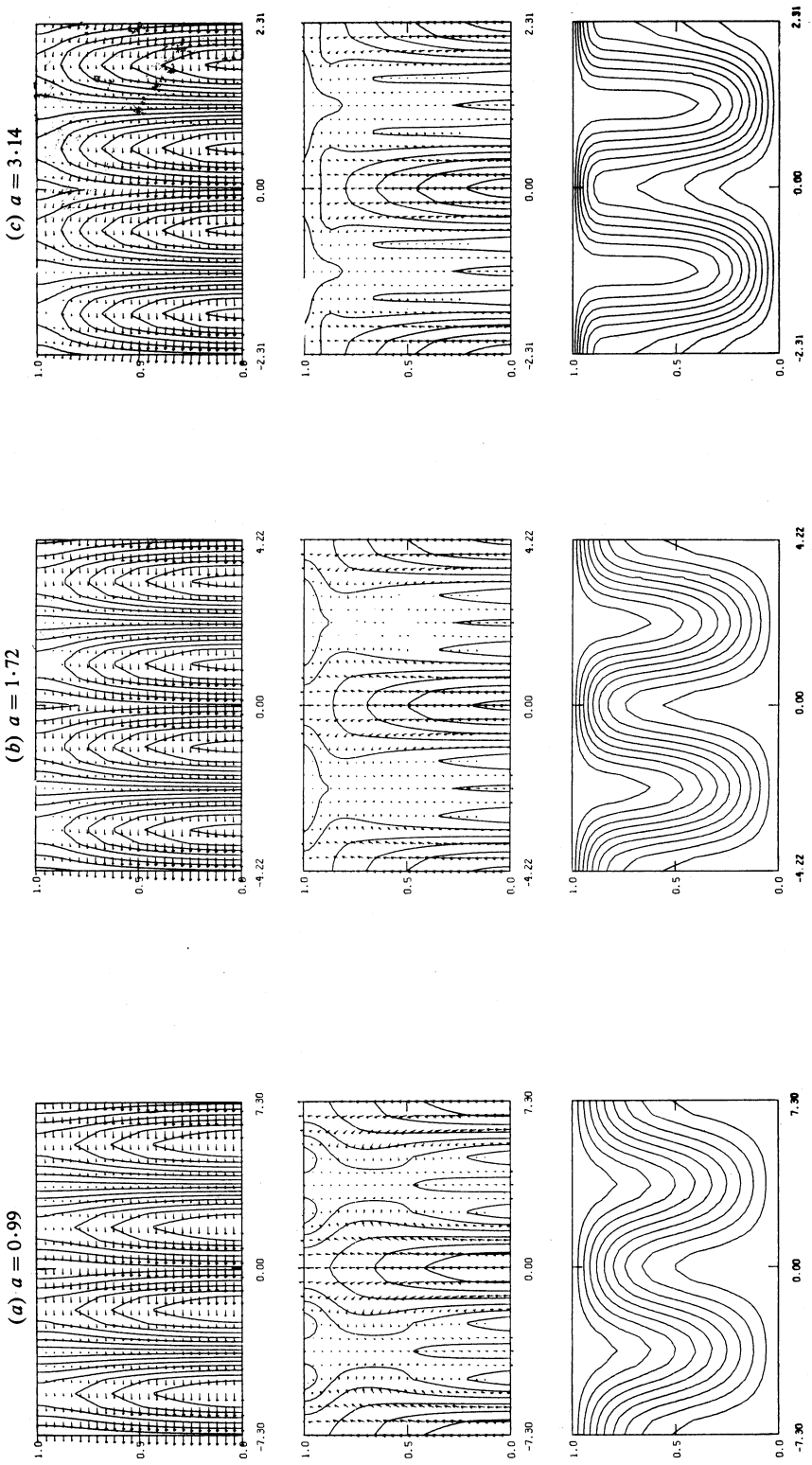

Fig. 6. Projections onto the x–z plane at $y = a/4$ for type II solutions of the velocity vectors together with contours of $|\boldsymbol{u}|$ (*top*), vorticity vectors together with contours of $|\nabla \times \boldsymbol{u}|$ (*middle*) and corresponding isotherms (*bottom*), for $R = 10^6$, $\sigma = 1{\cdot}0$ and the values of a indicated.

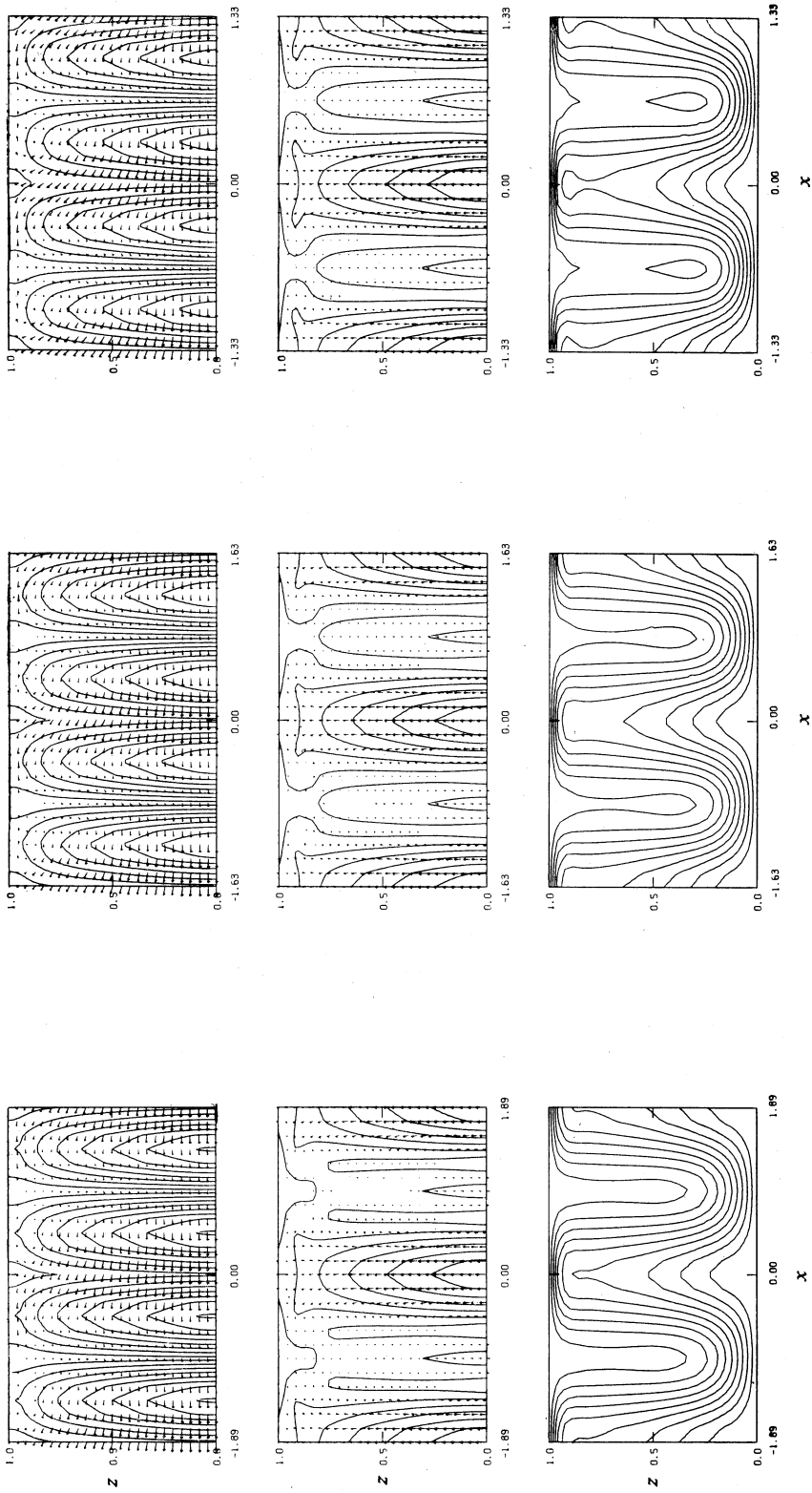

Figs 6*d*–6*f*.

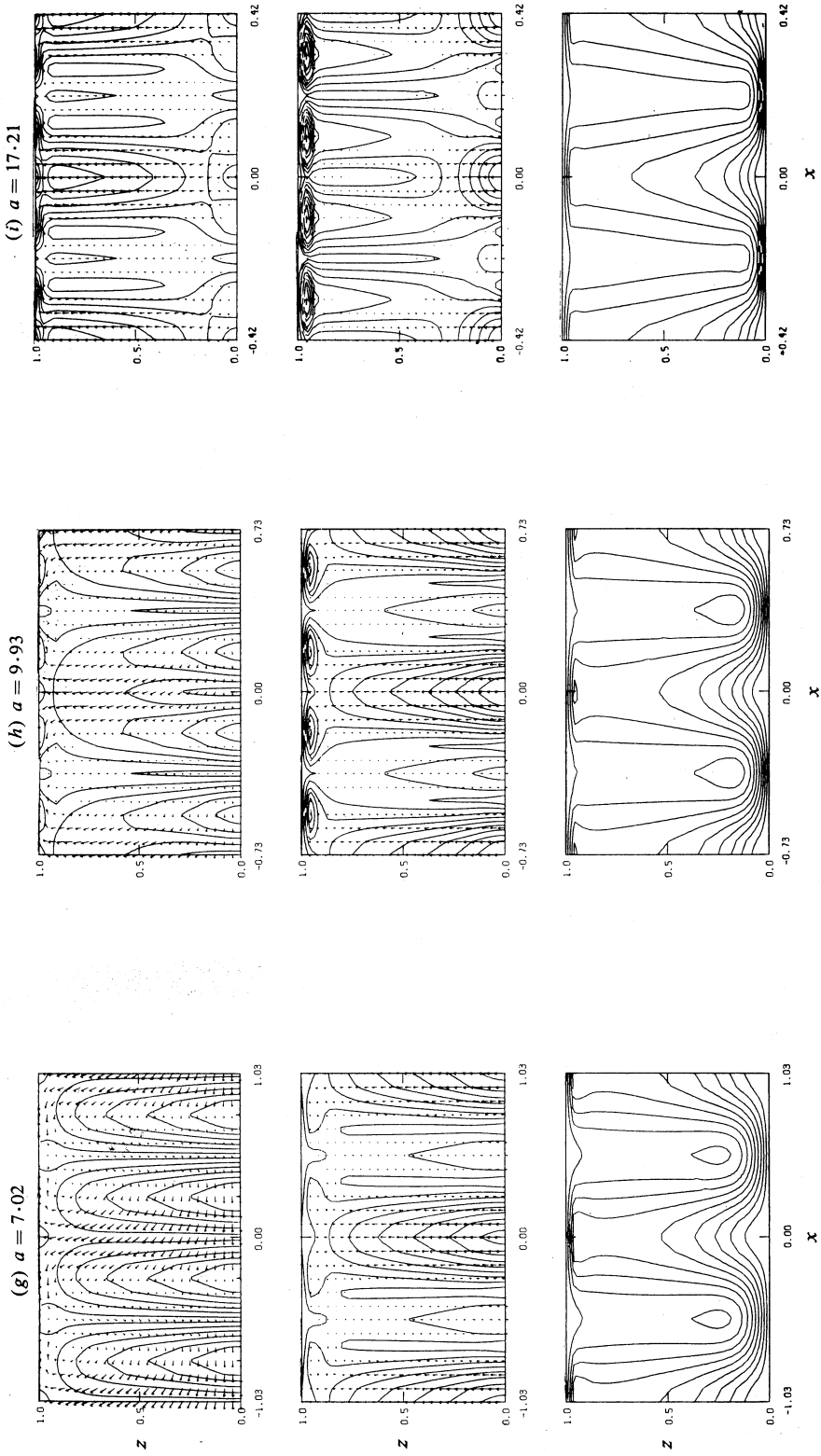

Figs 6*g*–6*i*.

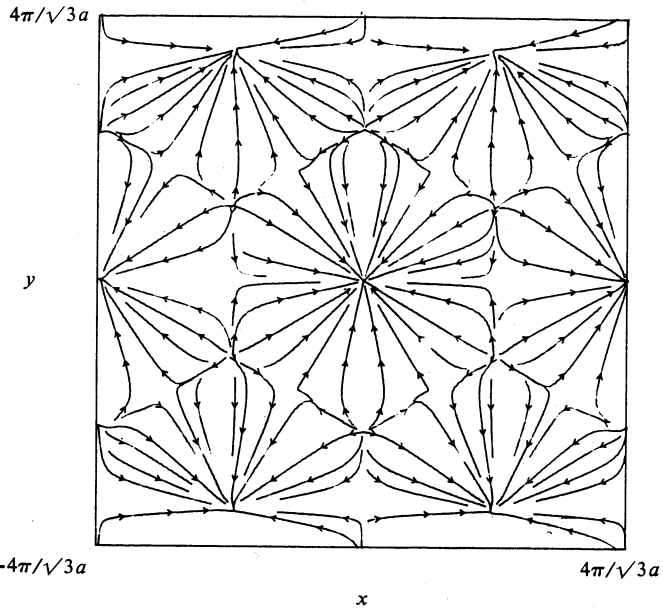

Fig. 7. Velocity streamlines at the top of layer, when the fluid descends at the centre of the cell, for type I solutions; these are independent of R and σ.

4. Conclusions

The results given above now demonstrate that for a given physical situation, described by the Rayleigh and Prandtl numbers, there can exist a continuous and bounded spectrum of horizontal wave numbers which permit two distinct non-trivial solutions of the system of single-mode equations (5)–(8) describing thermal convection in a fluid layer. In the present state, the theory offers no clear means for selecting one horizontal scale in preference to another, and yet it is clear from observations and experimental results that a selection mechanism prevails in Nature. At best, one could expect the fluid to transport heat in the most efficient and stable fashion.

As concluded by Murphy and Lopez (1984), the type II solutions, when they exist, are more stable than the corresponding type I solutions. In addition, this study has shown that the most efficient mode is not necessarily the most stable, and consequently there must be some form of physical compromise in the case of a single horizontal mode to determine the ultimate form of the convective state. Traditionally for type I solutions, this essentially meant that for given Rayleigh and Prandtl numbers, the preferred wave number corresponded to that which gave the largest heat flux as determined by the Nusselt number, but now, for a given set of R, σ and a, there exists the possibility of two distinct values of N, type I and type II. If this is the case, then the value of the horizontal wave number a which gives the largest N for type II solutions is expected to be the preferred length scale.

A time-dependent multi-mode analysis should give a clearer understanding of the selection mechanism for the preferred scales of motion, if it exists, as well as demonstrating the interaction between the different scales.

References

Chandrasekhar, S. (1961). 'Hydrodynamic and Hydromagnetic Stability' (Oxford Univ. Press).
Christopherson, D. G. (1940). *Quart. J. Math.* (*Oxford*) **11**, 63.
Herring, J. R. (1963). *J. Atmos. Sci.* **20**, 325.
Lopez, J. M., and Murphy, J. O. (1983). *Proc. Astron. Soc. Aust.* **5**, 173.
Malkus, W. V. R., and Veronis, G. (1958). *J. Fluid Mech.* **4**, 225.
Murphy, J. O. (1977). *Aust. J. Phys.* **30**, 177.
Murphy, J. O. (1980). *Proc. Astron. Soc. Aust.* **4**, 39.
Murphy, J. O., and Lopez, J. M. (1984). *Aust. J. Phys.* **37**, 179.
Toomre, J., Gough, D. O., and Spiegel, E. A. (1977). *J. Fluid Mech.* **79**, 1.

Manuscript received 2 March, accepted 21 June 1984